Halloysite nanoclay supported adsorptive removal of oxytetracycline antibiotic from aqueous media

Sammani Ramanayaka[a], Binoy Sarkar[b], Asitha T. Cooray[c,d], Yong Sik Ok[e,*], Meththika Vithanage[a,*]

[a] Ecosphere Resilience Research Center, Faculty of Applied Sciences, University of Sri Jayewardenepura, Nugegoda, Sri Lanka
[b] Department of Animal and Plant Sciences, The University of Sheffield, Western Bank, Sheffield, S10 2TN, UK
[c] Department of Chemistry, University of Sri Jayewardenepura, Nugegoda, Sri Lanka
[d] Instrument Center, Faculty of Applied Sciences, University of Sri Jayewardenepura, Nugegoda, Sri Lanka
[e] Korea Biochar Research Center, O-Jeong Eco-Resilience Institute (OJERI) & Division of Environmental Science and Ecological Engineering, Korea University, Seoul 02841, South Korea

GRAPHICAL ABSTRACT

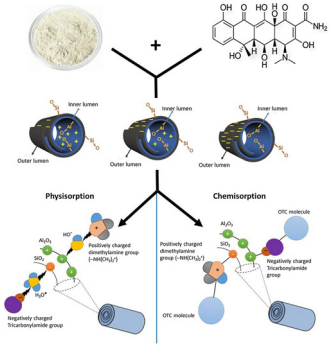

ARTICLE INFO

Editor: D. Aga

Keywords:
Emerging contaminants
Nanomaterials
Pharmaceuticals
Adsorption
Water pollution

ABSTRACT

Halloysite nanoclay was utilized to retain aqueous oxytetracycline (OTC) which is extensively used in the veterinary industry. The micro-structure and functionality of the nanoclay were characterized through spectroscopic techniques before and after adsorption. The OTC removal experiments were performed at different pH conditions (pH 3.0–9.0), ionic strengths (0.001, 0.01, 0.1 M $NaNO_3$) and contact time (up to 32 h) at an initial 25 mg/L OTC concentration with 1.0 g/L halloysite. Oxytetracycline adsorption was pH dependent, and the best pH was observed in the range of pH 3.5–5.5 at a 0.001 M ionic strength. At pH 3.5, the maximum OTC adsorption amount was 21 mg/g which translated to 68% removal of the initial OTC loading. Positively charged inner lumen and negatively charged outer lumen of the tubular halloysite structure led to form inner-sphere complexes with the anionic and cationic forms of OTC, respectively. A rapid adsorption of OTC was observed in the kinetic study where 62% OTC was adsorbed in 90 min.. Pseudo-second order equation obeyed by the kinetic data indicated that the adsorption was governed by chemisorption, whereas Hill isotherm equation was the most fitted with a maximum adsorption capacity of 52.4 mg/g indicating a cooperative adsorption phenomenon.

1. Introduction

Emerging contaminants released into the environment through various anthropogenic activities directly contaminate the water bodies and impair the quality of water. Due to extensive use by humans and in veterinary industry, antibiotics are among the commonly occurring pharmaceutical contaminants released from non-point and point sources, and are detected in elevated concentrations in ground and surface waters as emerging contaminants (Ding et al., 2012). Antibiotics exhibit a poor capability of absorption (30%) in the digestive tract, and the residues are released into the environment via the body excreta (Daghrir and Drogui, 2013). Contamination of manures with antibiotics has become a serious issue, especially in countries which have an agriculture and livestock-based economy (Ocampo-Pérez et al., 2012). Due to the direct application of manure or wastewater sludge to the agricultural fields, residuals of antibiotics flush off to the aquatic environment through surface runoff (Wang et al., 2016). In addition to the veterinary use, antibiotics are discharged at household level and through hospital wastewater. Conventional water treatment plants are in a limited capacity to remove antibiotics in the wastewaters. Therefore, antibiotics in waters have become a serious concern, and are considered as a threat of building up resistance in pathogenic microorganisms (Li et al., 2019). Hence, removing antibiotics from the aquatic environment has become a globally imperative necessity.

Among a variety of antibiotics that are commonly used, tetracyclines (TC) are one of the well-known and widely used groups. They are mainly used as a medicine for both human and animal infections, growth promoter and a food additive for livestock (Harja and Ciobanu, 2018). Among the TC-based antibiotics, oxytetracycline (OTC) is a regularly used broad-spectrum veterinary drug which acts against both gram-positive and gram-negative bacteria (Chopra and Roberts, 2001). Oxytetracycline is a hydrophilic molecule which consists of four fused benzene rings with multiple functional groups such as tertiary amino-, hydroxyl- and amide- groups. Speciation of OTC molecule occurs with the protonation and deprotonation of ionizable functional groups at different solution pH values. Therefore, OTC shows zwitterionic behavior in the range of solution pH from 3.5 to 7.5. The cationic and anionic forms of OTC is predominant at pH less than 3.5 and higher than 7.5, respectively (Premarathna et al., 2019). In aquatic environments, depending on the chemistry of the solution, OTC exhibits half-life time in the range of 6 h to 9 days, and results in transformation products such as 4-epi-oxytetracycline and α-apo-oxytetracycline via hydrolysis following first-order kinetics (Harja and Ciobanu, 2018). The predominance of OTC is influenced by different processes such as adsorption to solid phases, complexation with metals, oxidation, and hydrolysis reactions (Karpov et al., 2018).

In natural aquatic environments, OTC has been detected at micro concentration levels (μg/L) in surface water, wastewater and treated wastewater (Wang et al., 2016; Naik et al., 2017). Environmental monitoring studies have reported OTC as high as 68 μg/L in river water in Japan (Fatta-Kassinos et al., 2011). The guideline value of OTC in water is < 1 μg/L as recommended by the World Health Organization (WHO, 2012). Various attempts have been taken to remove OTC from waters using adsorption techniques due to significant removal capacities of different adsorbents, low cost and easy operation of the process. In selecting an adsorbent, one should carefully consider its OTC adsorption capacity, applicability under practical operating conditions, cost effectiveness and potential chances of creating a secondary environmental toxicity. Adsorption experiments are in general conducted with high concentrations of adsorbate in order to assess the capacity of the material so that it can be used for a long time as the environmental presence of contaminants are in minute amounts. Natural clay minerals, engineered nanomaterials, biochar, etc. have been considered as efficient adsorbents for OTC removal (Gao et al., 2012), while layered and tubular nanoclays have received recent attention due to their non-toxic nature, cost efficiency and easy modification procedures (Karpov et al., 2018; Lazzara et al., 2018).

Among various nanomaterials, halloysite nanoclay has been identified as a nanocontainer for smart coating applications (Zahidah et al., 2017), nanocarrier for herbicides (Zeng et al., 2019), and slowly releasing drug materials (Tan et al., 2014). However, limited attention has been received toward halloysite as an adsorbent for the removal of aquatic antibiotics (Duan et al., 2018; Xie et al., 2016). Halloysite nanoclay (HNC) is a naturally occurring porous clay mineral which can be seen in impure forms mixed with kaolinite, montmorillonite and other clay minerals. The porous halloysite nanoclay consists of 10–15 bilayers of aluminosilicate rolled into a cylinder or tubular structure having a length of 1–5 μm, and external and internal diameters of 40–60 nm and 10–15 nm, respectively (Ramadass et al., 2019). In the structure of halloysite, Si and O atoms are bound together forming a fused siloxane tetrahedral sheet and an edge-shared octahedral sheet made up of aluminum and hydroxide. The two-dimensional sheets are rolled-in to give an external siloxane (Si-O-Si) surface and an internal aluminol (Al-OH) surface to the nanotube, and it shows the structure of a multi-wall nanotube where the layers are separated by a monolayer of water molecules (Yuan et al., 2015). Pristine halloysite and its composites have been used as an adsorbent for removing antibiotics (e.g., ciprofloxacin) (Duan et al., 2018), heavy metals (e.g., As(v), Pb(II)) (Anastopoulos et al., 2018), dyes (e.g., Rhodamine 6 G cationic and Chrome azurol S anionic dyes) (Xu et al., 2019) and nanoparticles (e.g., Ag nanoparticles) (Janacek et al., 2018). Halloysite exhibited removal capacities to the tune of 21.7 mg/g for ciprofloxacin (Duan et al., 2018), 23.1 mg/g for Pb(II) ions (Anastopoulos et al., 2018), 43.6 mg/g for Rhodamine 6 G, 38.7 mg/g for Chrome azurol S (Zhao et al., 2013) and 67.9 mg/g for Ag nanoparticles (Janacek et al., 2018). However, the potential of HNC for antibiotics or OTC removal has not been studied in detail as has been done with other engineered nanoclays such as montmorillonite (Karpov et al., 2018). Therefore, the objectives of this study are to assess the OTC removal potential of HNC from aquatic environments under different environmental conditions, and postulate mechanisms behind the adsorption.

2. Materials and methods

2.1. Material characterization

Halloysite nanoclay and OTC were purchased from Sigma-Aldrich Co. Ltd. (USA). The topography and morphology of the pristine halloysite were investigated by a Field Emission Scanning Electron Microscope (FE-SEM), Hitachi SU6600 Analytical Variable Pressure FE-SEM (Japan). The crystalline structure of the pristine halloysite and OTC loaded halloysite was determined by Powder X-ray Diffraction (PXRD) by collecting the patterns on a Rigaku, Ultima IV X-ray Diffractometer (Japan) using Cu Kα radiation at a wavelength of 1.54056 Å in the scanning range of 10-60° (2θ) with a scanning speed of 2°/min. Surface functional groups of the halloysite, OTC and OTC-loaded halloysite were determined by KBr pellet method with Fourier Transform Infrared Spectrometer (FT-IR) (Thermo Scientific Nicolet iS10, USA) in the wavelength range of 4000–550 cm^{-1}. Solution pH values were measured with a pH meter (Adwa AD1030, Romania).

2.2. Edge experiments

The HNC was hydrated for 4 h on a magnetic stirrer after purging with high purity N_2 for 30 min and the concentration of OTC was kept as 25 mg/L in the suspension at a halloysite dosage of 1 g/L, with a total reaction volume of 100 mL. The variation of OTC adsorption to halloysite at room temperature (303 K) was studied within the pH range of 3.0–9.0 at different ionic strengths (0.1, 0.01 and 0.001 M $NaNO_3$). HNO_3 and NaOH (0.1 M) were used to adjust the solution pH values. The edge adsorption process was carried out for overnight on a shaker (100 rpm). Finally, the suspensions were filtered out through a syringe

filter (0.2 μm), and the absorbance values of the clear solutions were measured at the wavelength of 274 nm (Chi et al., 2010) using a UV–vis spectrophotometer (Shimadzu UV160A).

The OTC adsorption capacity q_t (mg/g) of halloysite at a specific time 't' (min) was calculated using the following equation:

$$q_t = \frac{(C_0 - C_t)V}{W} \quad (1)$$

where initial concentration C_o (mol/L), concentration C_t (mol/L) after time 't', volume of OTC solution V (L) and weight of halloysite W (kg).

2.3. Kinetic experiments

The adsorbent dosage and OTC concentrations were set similar as explained in the edge experiments. The pH values of the systems were in the range of pH 4.0–5.0 at an ionic strength of 0.001 M $NaNO_3$ based on the results from the edge experiment. The suspension was pipetted out at different time intervals from 2 to 1440 min. The pH value of each fraction was measured in the filtrate.

2.4. Isotherm experiments

Experiments to assess the effect of initial adsorbate concentrations on OTC adsorption were carried out at 303 K and pH = 4.75 in 0.001 M $NaNO_3$ solution. Oxytetracycline concentrations were maintained in the range of 10–500 mg/L for adsorption isotherm experiments at 1 g/L adsorbent dosage. The adsorbate was added into the system after 4 h of hydration of the adsorbent, and then a 12 h contact time (time taken to reach an equilibrium as observed from the kinetic experiment) was maintained. The suspensions were centrifuged at 8000 rpm for 20 min. Finally, the supernatant was filtered and analyzed for OTC concentrations, as discussed above.

2.5. Experimental data modeling

Origin 6.0 software was used for kinetic and isothermal modeling of the adsorption data to evaluate the maximum adsorption capacity of OTC and equilibrium time. In the kinetic modeling, pseudo first order (Eq.2), pseudo second-order (Eq. 3), Elovich (Eq. 4) and intra-particle diffusion (Eq. 5) models were tested for the curve fitting. The model giving the best fit to the data was determined from the correlation coefficient (R^2) and Chi^2 values. The equilibrium time and maximum OTC adsorption capacity by HNC were determined from the best fitted model.

$$\text{Pseudo first order: } \frac{dq_t}{dt} = k_1(q_e - q_t) \quad (2)$$

$$\text{Pseudo second order: } \frac{dq_t}{dt} = k_2(q_e - q_t)^2 \quad (3)$$

$$\text{Elovich equation: } \frac{dq_t}{dt} = \alpha\exp(-\beta qt) \quad (4)$$

$$\text{Intra-particle diffusion equation: } q_t = k_p t^{0.5} + C \quad (5)$$

where, the adsorbed amount of OTC at the equilibrium time (t) is q_t (mg/g), equilibrium adsorption capacity q_e (mg/g), initial adsorption rate, α (mg/g.min), Elovich constant, β (g/mg) while equilibrium rate constants are k_1 (/min) and k_2 (g/mg.min).

Classical adsorption isotherm models were used to understand the adsorption mechanisms and adsorbate-adsorbent binding interactions (Almasri et al., 2019). The Hill (Eq. 6), Freundlich (Eq. 7) and Temkin (Eq. 8) models were applied to the experimental data, and adsorption isotherms were obtained by plotting equilibrium concentrations (mg/L) vs. adsorption amounts (mg/g). The binding ability of different species onto homogeneous substrates can be described by the Hill isotherm model (Eq. 6). This model assumes that adsorption is a cooperative phenomenon with adsorbates at one site of the adsorbent influencing different binding sites on the same adsorbent (Farouq and Yousef, 2015). The Freundlich isotherm (Eq. 7) is more appropriate to heterogeneous surfaces and applied to multilayer complexation where it assumes the surface of the adsorbent is heterogeneous, and active sites and their energies distribute exponentially (Garcıa et al., 2004). The adsorption energy exponentially decreases with surface complexation from stronger to weak binding sites until the process is completed (Ayawei et al., 2015). The indirect effects of adsorbate-adsorbent interactions in the adsorption process are justified by using the Temkin isotherm model (Eq. 8) (Ringot et al., 2007). Temkin model mostly satisfies only for an intermediate range of adsorbate concentrations (Shahbeig et al., 2013).

$$\text{Hills isotherm: } q_{ads} = \frac{q_{max}\, c_e^{n_H}}{K_D + C_e^{n_H}} \quad (6)$$

$$\text{Freundlich isotherm: } q_e = K_f C_e^n \quad (7)$$

$$\text{Temkin isotherm: } q_{ads} = RT\frac{(lnAC_e)}{b} \quad (8)$$

where, K_f (mg/g)/(mg/L)^n is the Freundlich affinity parameter, while K_D and n_H are Hill constants. A and b are constants for the Temkin model, q_e (mg/g) is the equilibrium adsorption capacity for the Freundlich model and q_{ads} (mg/g) is the equilibrium adsorption capacity of Temkin model. C_e (mg/L) is the equilibrium liquid phase concentration, n is the Freundlich constant related to adsorption, R and T (K) are the universal gas constant and absolute temperature, respectively. The Hill cooperative coefficient of the binding is denoted as n_H.

3. Results and discussion

3.1. Scanning electron microscopic analysis (SEM)

The SEM images of HNC with two different magnifications (100 and 50 k) are shown in Fig. 1. Microscopic morphologies and the tubular structure were revealed with a length and a diameter of < 1 μm and 50–150 nm, respectively. Occasional aggregates due to static electrical charges among the nanotubes could also be seen in the images (Koh and

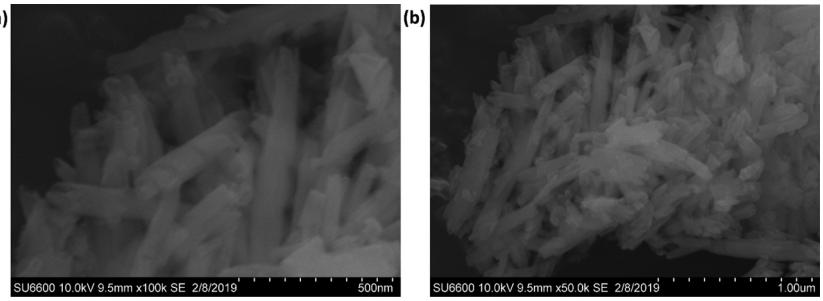

Fig. 1. SEM images of halloysite nanotubes and their occasional aggregates; (a) magnification x100 k, and (b) magnification x50 k.

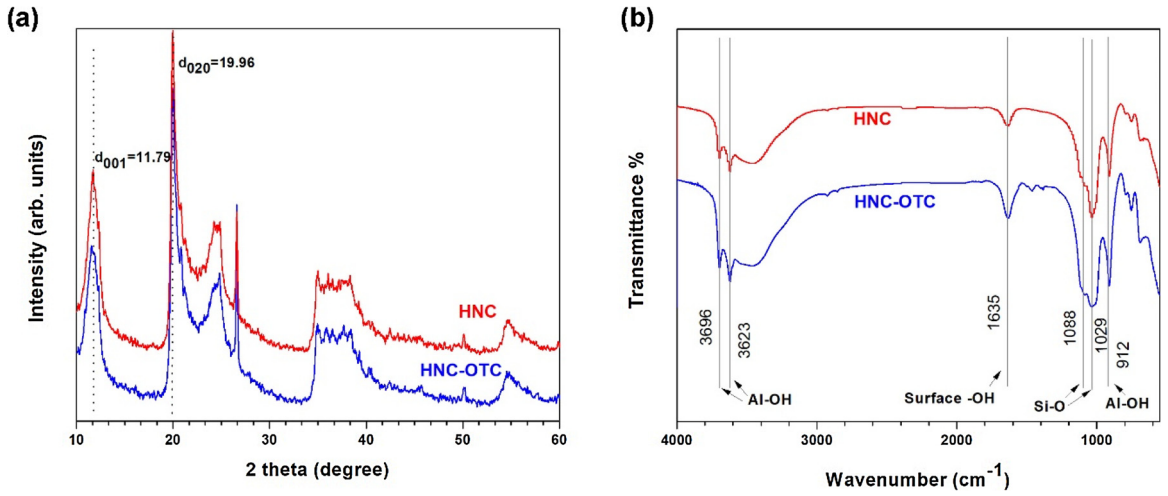

Fig. 2. (a) PXRD patterns of pristine halloysite (HNC), and OTC-loaded halloysite (HNC-OTC), and (b) FTIR spectra of pristine halloysite (HNC), and OTC-loaded halloysite (HNC-OTC).

Cheng, 2014).

3.2. Powder X-ray diffraction analysis (PXRD)

According to the PXRD patterns, the pristine halloysite [Fig. 2(A)] illustrated reflection peaks at diffraction angles: 2θ = 11.79°, 19.96°, 24.63°, 35.01°, 36.67° and 38.11° corresponding to the characterization indices of halloysite at (001), (020), (004), (130), (201) and (132) diffraction planes (Senoussi et al., 2016). A basal spacing (001) of 7.49 Å (2θ = 11.79°) was detected for the pristine halloysite nanoclay. A slight change in the basal spacing (7.51 Å) was observed in the PXRD pattern of OTC-adsorbed halloysite sample. Not any significant difference between pristine halloysite and OTC loaded halloysite was observed due to the adsorption of OTC only on the surface of nanotubes and the less space in between the tubular structure walls of the multilayer nanotube compared to layered structure clay minerals (Vinokurov et al., 2017).

3.3. Fourier transform infra-red analysis (FTIR)

The demonstration of FTIR analysis illuminates the surface functional groups of both pristine HNC and OTC loaded HNC. The bands centered at 3696 and 3623 cm^{-1} corresponded to outer surface O—H and inner surface OH— stretching vibrations of Al—OH groups (Fig. 2) (Zhang and Yang, 2012). The characteristic bands, O—H stretching of intercalated water, O—H deformation of water and Si–O stretching vibration bands, were observed at 3448 cm^{-1} and 1635 cm^{-1} and 1029 cm^{-1}, respectively (Kurczewska et al., 2019). The band appearing at 1088 cm^{-1} represented Al-O stretching vibration, while the band at 912 cm^{-1} was attributed for OH bending. The weak band at 744 cm^{-1} confirmed the —OH translational vibrations of halloysite (Christoforidis et al., 2016). The bands between 2800-2900 cm^{-1} depicted the presence of organic compounds, which is known as acrylate that was used in clay processing. The peaks at 1620 cm^{-1} and 1447 cm^{-1} represented the NH— bond of $-CONH_2$ and the C=C vibrations of the skeletal aromatic rings of OTC molecule (Punamiya et al., 2013).

3.4. Oxytetracycline - halloysite interaction studies

3.4.1. Effect of pH and ionic strength on adsorption behavior

Adsorption pattern and capacity at different pH levels were investigated as the pH of the media is crucial for the surface complexation of OTC on HNC. The edge experiments demonstrated that the maximum adsorption of OTC to HNC was 21 mg/g at pH 3.5 (Fig. 3). It exhibited 84% removal capacity from the initial concentration. This data corroborated with reported literature on OTC adsorption by illite (Bansal, 2013). Further, it was observed that the adsorption of OTC at 0.001 M ionic strength had the least pH dependency in the pH range of 3.5 to 6.0. The point of zero charge (pHzpc) of HNC was determined to be pH 2.5 to 2.9 (Almasri et al., 2019; Vergaro et al., 2010). Based on the pHzpc data, halloysite surface showed an overall negative charge at the studied pH values during the experiment.

At the same time, the ionizable functional groups of OTC molecules can protonate or deprotonate based on the pH of the media (Fig. 3). Cationic form of OTC is predominant at pH < 3.5, the zwitterionic form prevails at the pH range of 3.5–7.5, and the anionic form becomes dominant at pH > 7.5 (Vaz, 2016). Therefore, considering the point of zero charge (pHzpc) of halloysite (pH 2.5), in the studied pH range (pH 3–9), positively charged dimethylamine group of zwitterion complexes would prevail on the deprotonated HNC surfaces. Therefore, the interaction of OTC with HNC might be suggested as a physisorption process through electrostatic and van der Wall's attractions (Duan et al., 2018; Almasri et al., 2019). The HNC has a tubular structure with a remarkable chemical composition where the exterior and interior of the tube is dominated by SiO_2 and Al_2O_3 groups (Yu et al., 2016). Interestingly, the inner lumen of the halloysite tube consists of Al_2O_3 with a positive charge at the pH range of 2.5–8.5 (Yuan et al., 2015). This might allow the selective adsorption of anionic tricarbonylamide in zwitterion form on the positively charged Al_2O_3 groups in the inner lumen (Almasri et al., 2019). The opposite might happen on the negatively charged SiO_2 surface in the outer lumen with positively charged dimethylamine groups of zwitterionic OTC, and this could be suggested as a mono-dentate chemisorption.

The edge experiments at different ionic strengths in the media indicated a slight ionic strength dependency of OTC complexation with HNC, especially at low and medium ionic strength levels (0.001 and 0.01 M with $NaNO_3$). However, a distinct ionic strength dependency was demonstrated in the 0.1 M $NaNO_3$ medium where the least amount of OTC adsorption was observed. There was about 50% reduction in the OTC adsorption capacity with 0.1 M $NaNO_3$ compared to 0.001 M $NaNO_3$ (Fig. 3) The ionic strength dependency of an adsorbate can be used for postulating the surface complexation mechanism (Duan et al., 2018). A marked effect observed on adsorption at different ionic strengths indicates outer sphere bonding, whereas no distinct separation of adsorption edges exhibits an inner sphere complexation of adsorbate to the adsorbent (Gu et al., 2018). In the case of OTC complexation to halloysite, a separation of adsorption edges was not readily discerned between 0.001 and 0.1 M $NaNO_3$ media indicating an inner

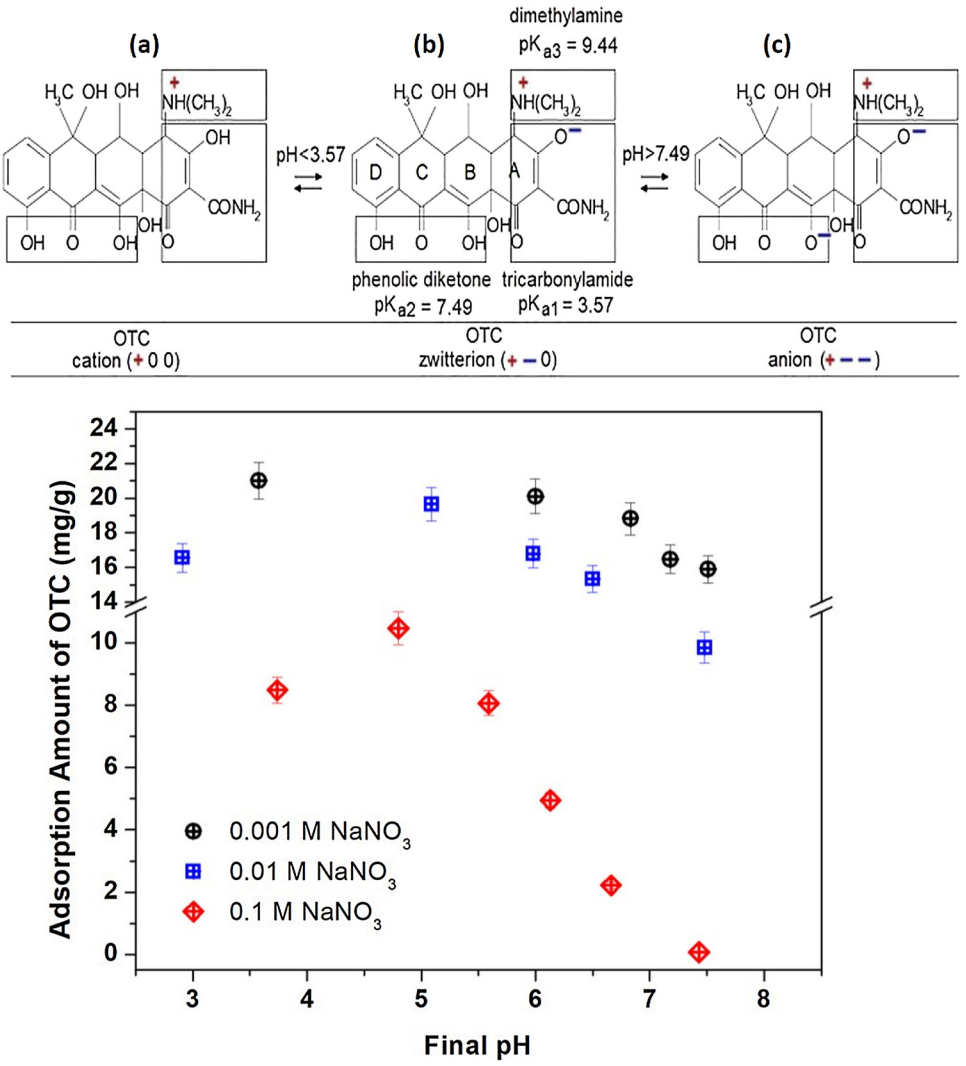

Fig. 3. Speciation of OTC: (a) cationic, (b) zwitterion, and (c) anionic forms, and the effect of pH on the adsorption amount of OTC on HNC at different ionic strengths (0.1, 0.01, 0.001 M with $NaNO_3$) in aqueous media. Initial OTC concentration was kept at 25 mg/L.

sphere complexation reaction was possibly taking place. However, a high electrolyte concentration (0.1 M $NaNO_3$) yielding distinctly separated adsorption edges suggested an outer sphere surface complexation of OTC too with the halloysite adsorbent.

3.4.2. *Effect of initial solution pH*

The distribution coefficient (K_D) values are strongly dependent on the solution pH and chemical speciation of OTC molecules (Vithanage et al., 2014). Fig. 4 revealed a minor increment of K_D values up to pH 6 above which the K_D values observed a significant decrease during the experimental ionic strengths. Interestingly, distribution coefficients expressed a reduction in their values with the increasing ionic strengths of the media which might be due to the ion exchange mechanism became predominant through the formation of outer sphere complex of OTC with unbalanced electrical charges within the halloysite framework. Furthermore, it has been understood that in the high ionic strength media, the extension of the double layer is insignificant and hence, permselectivity is low so that the ion exchange possibility is less. Therefore, in this experiment, high ionic strength indicated less adsorption. With the decrease in ionic strength, permselectivity is significant and, during the pHs where the surface is negatively charged, cations partition easily into the halloysite surface while anions are excluded and vice versa at lower ionic strengths (Smith et al., 2009; Chikkamath et al., 2018). The K_D values closely corroborated to those

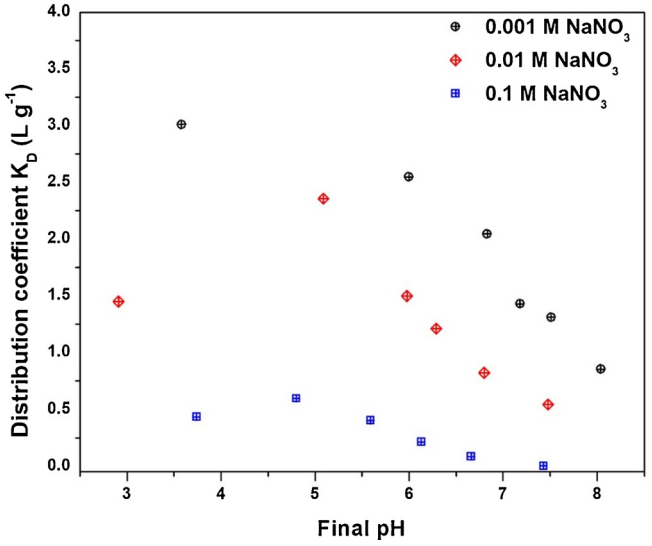

Fig. 4. Variation of distribution coefficients (K_D) in the pH range of 2.5–8.5 for OTC-loaded HNC.

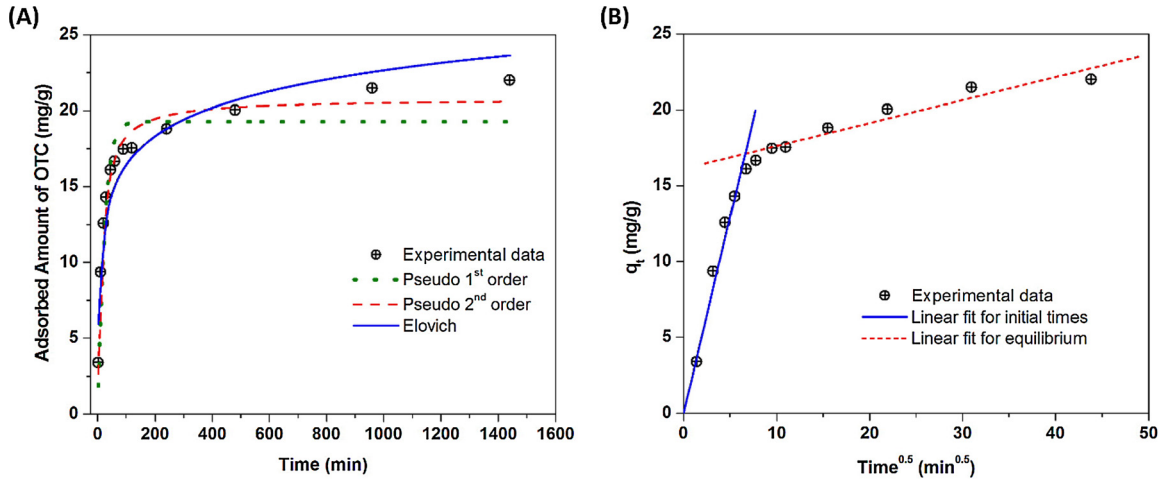

Fig. 5. (A) Influence of time on OTC removal by HNC at 1 g/L adsorbent dosage, background ionic strength of 0.001 M $NaNO_3$, at pH 4 with 25 mg/L OTC concentration, and kinetic data fit for Pseudo 1st order, Pseudo 2nd order and Elovich equations (B) Intra-particle diffusion model fitting for kinetic data. Symbols represent the experimental data where lines represent modeled data.

reported for OTC onto other clay adsorbents and polymers (Zhang et al., 2014). The distribution coefficients (K_D) represented the adsorption affinity of OTC on to the HNC and variation of K_D with pH approached the maximum value in the pH range of 5.5–7.5, where OTC is predominantly zwitterionic.

3.4.3. Kinetic effect on adsorption

The influence of time on OTC adsorption up to 24 h is shown in Fig. 5(A). A rapid adsorption was observed during the first 120 min reaching an adsorption capacity of 17.5 mg/g, which could be attributed to the retention of OTC within the large pores of HNC in the inner lumen. The removal of OTC indicated reaching equilibrium after 480 min. The amount of OTC adsorption at the equilibrium was only about 10% higher than that of after 120 min of the reaction.

Both pseudo-first-order and pseudo-second-order models were fitted well for the rapid stage of the adsorption reaction (Fig. 5a; Table 1). The best fit was observed for the pseudo-second order model with a correlation coefficient (R^2) value of 0.98. The R^2 value for the pseudo-first-order model was considerably lower (0.908) than that of the pseudo-second-order model (Table 1). At the same time, the Chi^2 and error values of the pseudo second-order model were lesser than that of the pseudo first order and Elovich models, indicating that the pseudo-second-order kinetic model best described the OTC adsorption process on HNC.

When the rate limiting step of adsorption is solely based on intraparticle diffusion, then the plot of qt vs. $t^{0.5}$ results a linear relationship that passes through the origin (Weber and Morris, 1963). In the current study, the linear plots for HNC-OTC system passed through the origin until 45 min [Fig. 5(B)] depicting that the intraparticle diffusion was involved as the rate-limiting factor at the beginning of the adsorption process. However, after 45 min, the adsorption process of the linear plot of qt vs. $t^{0.5}$ did not pass through the origin suggesting that the intraparticle diffusion was not the only rate-determining step in this case. Therefore, the kinetic data modeling of the HNC-OTC interaction illustrated both intraparticle diffusion and chemisorption as the mechanisms of adsorbate-adsorbent complexation.

3.4.4. Adsorption isotherm study

The equilibrium concentrations of OTC vs. adsorbed amounts is presented in Fig. 6. The amount of adsorbed OTC showed an increasing trend with the increment of initial OTC concentration. The availability of HNC surface sites was high at low initial OTC concentrations, and therefore, HNC exhibited almost 100% adsorption capacity until it reached the equilibrium at a concentration of 173.0 mg/L. When the availability of binding sites became less with the increasing initial concentrations of OTC, the adsorption amount became less.

Table 1
Kinetic and isotherm model parameters for the adsorption of OTC onto halloysite nanoclay at 1 g/L loading.

Experimentation	Model	Parameter	Value
Kinetic models	Pseudo first order	k_1 (per min)	0.908
		q_e (mg/g)	19.281
		R^2	0.658
		Chi^2	2.853
	Pseudo second Order	k_2 [g/(mg min)]	0.004
		q_e (mg/g)	20.78
		R^2	0.980
		Chi^2	0.624
	Elovich	α_E [mg/(g min)]	12.25
		β_E (g/mg)	0.371
		R^2	0.933
		Chi^2	2.072
Isotherm models	Hill	K_D	0.002
		n_H	0.246
		q_{max} (mg/g)	52.38
		R^2	0.913
		Chi^2	7.406
	Freundlich	K_f (mg/g)/(mg/L)^n	9.426
		n	0.165
		R^2	0.910
		Chi^2	6.786
	Temkin	A	8.787
		b	2.642
		R^2	0.909
		Chi^2	5.824
	Langmuir	q_{max} (mg/g)	22.42
		K (L/mg)	0.567
		R^2	0.808
		Chi^2	12.34

The experimental data of HNC-OTC interaction was best fitted to the Hill equation given the highest correlation coefficient (R^2) of 0.913 (Table 1). The Hill isotherm model hypothesizes the binding of different species onto homogeneous substrates and the ability of binding ligands at one site of the adsorbent macromolecule influences different binding sites on the same adsorbent macromolecule, which is a cooperative phenomenon (Farouq and Yousef, 2015). Three possibilities of binding could occur in this model: $n_H > 1$ giving positive cooperative binding, $n_H = 1$ giving non-cooperative or hyperbolic binding, and $n_H < 1$ giving negative cooperativity of binding (Saadi et al., 2015). The HCN-OTC experimental data fitting with the Hill isotherm equation

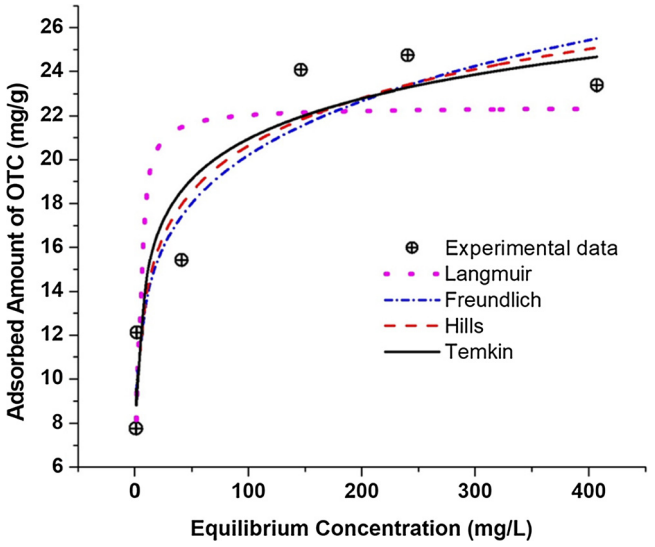

Fig. 6. Experimental data of initial OTC concentrations vs. adsorption amounts at pH = 4, background ionic strength = 0.001 M $NaNO_3$, and 1 g/L halloysite dosage. Symbols represent experimental data, whereas lines indicate modeled data using non-linear least square fit of Langmuir, Freundlich, Hills and Temkin equations.

exhibited a negative cooperativity, which indicates binding of the first ligand of OTC reduces the probability of binding for a second OTC molecule and at the same time $n_H < 1$ depicts the existence of macromolecules with multiple binding site and different ligand affinities (Cattoni et al., 2015). The maximum OTC adsorption capacity calculated from the Hill isotherm model was 52.4 mg/g. Modeling of data resulted in a decent fit to Freundlich (R^2 = 0.910) and Temkin (R^2 = 0.909) equations also (Table 1). However, the least fit was observed for the Langmuir equation (R^2 = 0.808) (Table 1). Fit to the Freundlich model depicted heterogeneity of the halloysite surface due to the presence of Al_2O_3 and SiO_2 sites, and indicated the possibility of multilayer complexation (Kurczewska et al., 2019). The model calculated values of n in the Freundlich equation was higher than unity indicating an unfavorable adsorption (Mayakaduwa et al., 2016). Furthermore, fit to the Temkin equation postulated that the adsorption energy was uniformly distributed at the HNC surface, and the heat of adsorption of surface molecules was reduced linearly (Kumar et al., 2010).

3.5. Confirmation of OTC-HNC interaction

Oxytetracycline adsorption on to HNC could be confirmed from the FTIR and PXRD data (Fig. 2). The peaks at 1620 cm^{-1} and 1447 cm^{-1} represented the NH− bond of −CONH and the C=C vibrations of the skeletal aromatic rings of OTC molecule, and these particular peaks in HNC-OTC FTIR spectrum represented the adsorption of OTC. The outer surface O−H and inner surface OH− stretching vibrations of Al−OH groups (3696 and 3623 cm^{-1}) and −OH bending at 912 cm^{-1} comprehended a slight increment in the peak length due to the binding of −OH groups from OTC. The N−H bonds of $-CONH_2$ and the C=C vibrations of the skeletal aromatic rings of OTC molecule attributed by the peaks at 1620 cm^{-1} and 1447 cm^{-1} and the presence of these peaks confirmed the adsorption od OTC (Kurczewska et al., 2019). In PXRD analysis, slight peak shift from 2θ = 24° to 2θ = 25° revealed the adsorption of OTC on to HNC surfaces.

4. Conceivable adsorption mechanisms

Oxytetracycline is sensitive to solution pH and easily protonated at pH < 3.5 where it exists in the cationic form. Beyond pH 7.5, the anionic form is predominant, and zwitterionic form is dominant in the pH range of 3.5–7.5 (Premarathna et al., 2019). At low pH values (pH 2.9–3.5), a cationic form of OTC complexes with negatively charged HNC (pHzpc = 2.9) via electrostatic interaction, which is a non-specific adsorption (Vergaro et al., 2010; Mellouk et al., 2009) (Fig. 7). Beyond the solution pH of 3.5, the cationic dimethylamine species may electrostatically complex with the anionic surface of HNC. Therefore, electrostatic complexation would be prominent between HNC and OTC during the adsorption process at the experimental pH conditions (Duan et al., 2018). Furthermore, at the low pH conditions, an increase in the final pH value was observed during the experimental process, which suggested an ion exchange with the hydroxide ligands on the surface might also occur. Beyond pH 7.5, both OTC and HNC surface is negatively charged, and hence electrostatic repulsion reduces the OTC-HNC interaction (Almasri et al., 2019).

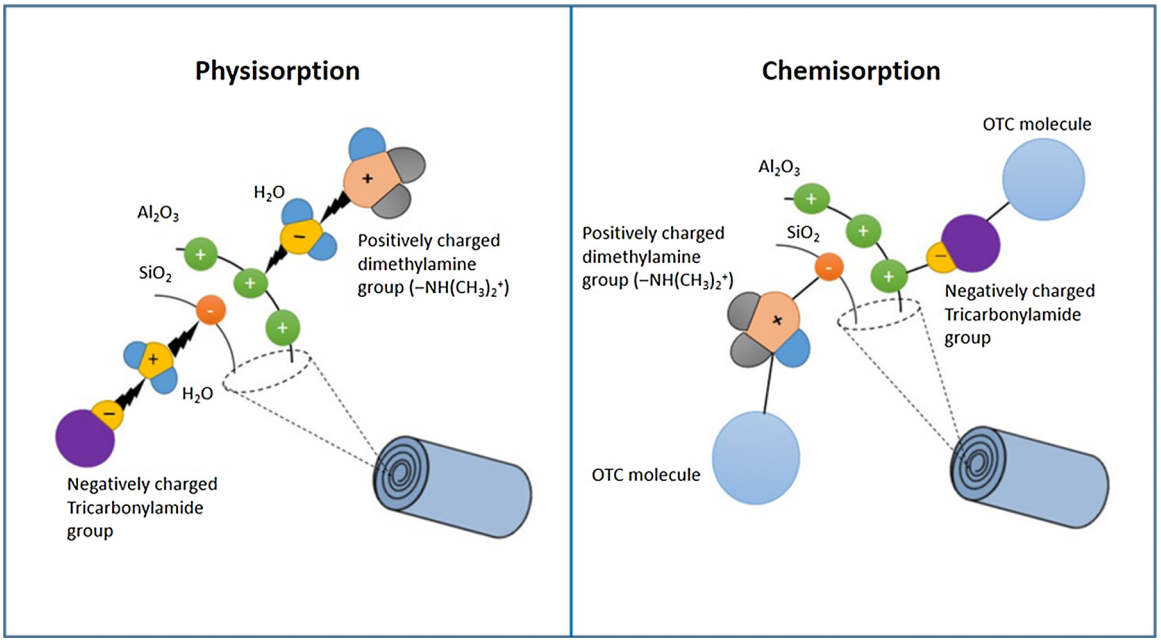

Fig. 7. Schematic diagram of surface complexation of oxytetracycline, to charged surface of halloysite tubular structure through physisorption and chemisorption.

Moreover, positively charged Al_2O_3 groups and the negatively charged SiO_2 groups in the inner and outer lumens of HNC allows chemisorption with the tricarbonylamide and dimethylamine in the zwitterionic form of OTC. A strong covalent bond may form through monolayer complexation of the OTC directly to the surface without a water molecule intervened in between pH 2.5–8.0, which is specific adsorption (Almasri et al., 2019). Time influence for OTC adsorption recommended chemisorption mechanism (Fig. 7). Isotherm data modeling indicates cooperative adsorption phenomenon with OTC binding at different surface sites of halloysite (Aharoni and Ungarish, 1977). Multilayer complexation has been illustrated by the isotherm fitting to Freundlich and Temkin equations. Further, Freundlich fit with $n < 1$ denotes a weak affinity of OTC to halloysite surface sites demonstrating non-specific adsorption.

5. Conclusions

In this study, removal of oxytetracycline antibiotic from aqueous media by using halloysite nanoclay has been reported. Confirmation of successful adsorption of OTC onto HNC surface has been explored with scanning electron micrographs, x-ray diffractograms, and FTIR spectrographs. Edge experiment indicated that the OTC adsorption to HNC was pH dependent via both specific and non-specific adsorption. OTC removal was high in the pH range of 3.5–5.0 with 12 h as the equilibrium time to reach the maximum adsorption. Ionic strength edge data indicated inner-sphere complexation in between 0.001 and 0.01 M $NaNO_3$ in the media. Within the first 30 min, more than 50% of OTC was removed whereas kinetic modeling indicated chemisorption and intraparticle diffusion as the rate limiting step in the adsorption process. Isotherm data were fitted best with Hill equation describing cooperative adsorption of OTC to halloysite. The calculated maximum adsorption capacity was given as 52.4 mg/g that demonstrated halloysite to be a potential sorbent for the removal of OTC from aqueous media.

Acknowledgements

Authors acknowledge Instrument Center of Faculty of Applied Sciences for providing analytical facilities and Research Council for providing funding for the research student.

References

Aharoni, C., Ungarish, M., 1977. Kinetics of activated chemisorption. Part 2.—theoretical models. J. Chem. Soc. Faraday Trans. 1 Phys. Chem. Condens. Phases 73, 456–464.
Almasri, D.A., Saleh, N.B., Atieh, M.A., McKay, G., Ahzi, S., 2019. Adsorption of phosphate on iron oxide doped halloysite nanotubes. Sci. Rep. 9, 3232. https://doi.org/10.1038/s41598-019-39035-2.
Anastopoulos, I., Mittal, A., Usman, M., Mittal, J., Yu, G., Núñez-Delgado, A., Kornaros, M., 2018. A review on halloysite-based adsorbents to remove pollutants in water and wastewater. J. Mol. Liq. 269, 855–868. https://doi.org/10.1016/j.molliq.2018.08.104.
Ayawei, N., Angaye, S.S., Wankasi, D., Dikio, E.D., 2015. Synthesis, characterization and application of Mg/Al layered double hydroxide for the degradation of congo red in aqueous solution. Open J. Phys. Chem. 5, 56.
Bansal, O.P., 2013. Sorption of tetracycline, oxytetracycline, and chlortetracycline in illite and kaolinite suspensions. ISRN Environ. Chem. 2013.
Cattoni, D.I., Chara, O., Kaufman, S.B., González Flecha, F.L., 2015. Cooperativity in binding processes: new insights from phenomenological modeling. PLoS One 10https://doi.org/10.1371/journal.pone.0146043. e0146043–e0146043.
Chi, Z., Liu, R., Zhang, H., 2010. Potential enzyme toxicity of oxytetracycline to catalase. Sci. Total Environ. 408, 5399–5404.
Chikkamath, S., Patel, M.A., Kar, A.S., Raut, V., Tomar, B.S., Manjanna, J., 2018. Sorption of Eu (III) on Fe–montmorillonite relevant to geological disposal of HLW. Radiochim. Acta 106, 971–983.
Chopra, I., Roberts, M., 2001. Tetracycline antibiotics: mode of action, applications, molecular biology, and epidemiology of bacterial resistance. Microbiol. Mol. Biol. Rev. 65, 232–260.
Christoforidis, K.C., Melchionna, M., Montini, T., Papoulis, D., Stathatos, E., Zafeiratos, S., Kordouli, E., Fornasiero, P., 2016. Solar and visible light photocatalytic enhancement of halloysite nanotubes/gC 3 N 4 heteroarchitectures. RSC Adv. 6, 86617–86626.
Daghrir, R., Drogui, P., 2013. Tetracycline antibiotics in the environment: a review. Environ. Chem. Lett. 11, 209–227.
Ding, R., Zhang, P., Seredych, M., Bandosz, T.J., 2012. Removal of antibiotics from water using sewage sludge- and waste oil sludge-derived adsorbents. Water Res. 46, 4081–4090. https://doi.org/10.1016/j.watres.2012.05.013.
Duan, W., Wang, N., Xiao, W., Zhao, Y., Zheng, Y., 2018. Ciprofloxacin adsorption onto different micro-structured tourmaline, halloysite and biotite. J. Mol. Liq. 269, 874–881. https://doi.org/10.1016/j.molliq.2018.08.051.
Farouq, R., Yousef, N.S., 2015. Equilibrium and kinetics studies of adsorption of copper (II) ions on natural biosorbent. Int. J. Chem. Eng. Appl. 6, 319.
Fatta-Kassinos, D., Meric, S., Nikolaou, A., 2011. Pharmaceutical residues in environmental waters and wastewater: current state of knowledge and future research. Anal. Bioanal. Chem. 399, 251–275. https://doi.org/10.1007/s00216-010-4300-9.
Gao, Y., Li, Y., Zhang, L., Huang, H., Hu, J., Shah, S.M., Su, X., 2012. Adsorption and removal of tetracycline antibiotics from aqueous solution by graphene oxide. J. Colloid Interface Sci. 368, 540–546. https://doi.org/10.1016/j.jcis.2011.11.015.
Garcıa, G., Faz, A., Cunha, M., 2004. Performance of Piptatherum miliaceum (Smilo grass) in edaphic Pb and Zn phytoremediation over a short growth period. Int. Biodeterior. Biodegrad. 54, 245–250.
Gu, W., Li, X., Xing, M., Fang, W., Wu, D., 2018. Removal of phosphate from water by amine-functionalized copper ferrite chelated with La(III). Sci. Total Environ. 619–620, 42–48. https://doi.org/10.1016/j.scitotenv.2017.11.098.
Harja, M., Ciobanu, G., 2018. Studies on adsorption of oxytetracycline from aqueous solutions onto hydroxyapatite. Sci. Total Environ. 628, 36–43.
Janacek, D., Kvitek, L., Karlikova, M., Pospiskova, K., Safarik, I., 2018. Removal of silver nanoparticles with native and magnetically modified halloysite. Appl. Clay Sci. 162, 10–14. https://doi.org/10.1016/j.clay.2018.05.024.
Karpov, M., Seiwert, B., Mordehay, V., Reemtsma, T., Polubesova, T., Chefetz, B., 2018. Transformation of oxytetracycline by redox-active Fe(III)- and Mn(IV)-containing minerals: processes and mechanisms. Water Res. 145, 136–145. https://doi.org/10.1016/j.watres.2018.08.015.
Koh, B., Cheng, W., 2014. Mechanisms of Carbon Nanotube Aggregation and the Reversion of Carbon Nanotube Aggregates in Aqueous Medium. Langmuir. 30, 10899–10909. https://doi.org/10.1021/la5014279.
Kumar, P.S., Ramakrishnan, K., Gayathri, R., 2010. Removal of nickel (II) from aqueous solutions by ceralite IR 120 cationic exchange resins. J. Eng. Sci. Technol. 5, 232–243.
Kurczewska, J., Cegłowski, M., Schroeder, G., 2019. Alginate/PAMAM dendrimer – halloysite beads for removal of cationic and anionic dyes. Int. J. Biol. Macromol. 123, 398–408. https://doi.org/10.1016/j.ijbiomac.2018.11.119.
Lazzara, G., Cavallaro, G., Panchal, A., Fakhrullin, R., Stavitskaya, A., Vinokurov, V., Lvov, Y., 2018. An assembly of organic-inorganic composites using halloysite clay nanotubes. Curr. Opin. Colloid Interface Sci. 35, 42–50. https://doi.org/10.1016/j.cocis.2018.01.002.
Li, N., Zhou, L., Jin, X., Owens, G., Chen, Z., 2019. Simultaneous removal of tetracycline and oxytetracycline antibiotics from wastewater using a ZIF-8 metal organic-framework. J. Hazard. Mater. 366, 563–572.
Mayakaduwa, S.S., Kumarathilaka, P., Herath, I., Ahmad, M., Al-Wabel, M., Ok, Y.S., Usman, A., Abduljabbar, A., Vithanage, M., 2016. Equilibrium and kinetic mechanisms of woody biochar on aqueous glyphosate removal. Chemosphere 144, 2516–2521.
Mellouk, S., Cherifi, S., Sassi, M., Marouf-Khelifa, K., Bengueddach, A., Schott, J., Khelifa, A., 2009. Intercalation of halloysite from Djebel Debagh (Algeria) and adsorption of copper ions. Appl. Clay Sci. 44, 230–236.
Naik, L., Sharma, R., Mann, B., Lata, K., Rajput, Y.S., Nath, B.S., 2017. Rapid screening test for detection of oxytetracycline residues in milk using lateral flow assay. Food Chem. 219, 85–92.
Ocampo-Pérez, R., Rivera-Utrilla, J., Gómez-Pacheco, C., Sánchez-Polo, M., López-Peñalver, J.J., 2012. Kinetic study of tetracycline adsorption on sludge-derived adsorbents in aqueous phase. Chem. Eng. J. 213, 88–96.
Premarathna, K.S.D., Rajapaksha, A.U., Adassoriya, N., Sarkar, B., Sirimuthu, N.M.S., Cooray, A., Ok, Y.S., Vithanage, M., 2019. Clay-biochar composites for sorptive removal of tetracycline antibiotic in aqueous media. J. Environ. Manage. 238, 315–322.
Punamiya, P., Sarkar, D., Rakshit, S., Datta, R., 2013. Effectiveness of aluminum-based drinking water treatment residuals as a novel sorbent to remove tetracyclines from aqueous medium. J. Environ. Qual. 42, 1449–1459.
Ramadass, K., Singh, G., Lakhi, K.S., Benzigar, M.R., Yang, J.-H., Kim, S., Almajid, A.M., Belperio, T., Vinu, A., 2019. Halloysite nanotubes: novel and eco-friendly adsorbents for high-pressure CO2 capture. Microporous Mesoporous Mater. 277, 229–236. https://doi.org/10.1016/j.micromeso.2018.10.035.
Ringot, D., Lerzy, B., Chaplain, K., Bonhoure, J.-P., Auclair, E., Larondelle, Y., 2007. In vitro biosorption of ochratoxin A on the yeast industry by-products: comparison of isotherm models. Bioresour. Technol. 98, 1812–1821.
Saadi, R., Saadi, Z., Fazaeli, R., Fard, N.E., 2015. Monolayer and multilayer adsorption isotherm models for sorption from aqueous media. Korean J. Chem. Eng. 32, 787–799.
Senoussi, H., Osmani, H., Courtois, C., Bourahli, M. el H., 2016. Mineralogical and chemical characterization of DD3 kaolin from the east of Algeria, Boletín La Soc. Española Cerámica Y Vidr. 55, 121–126. https://doi.org/10.1016/j.bsecv.2015.12.001.
Shahbeig, H., Bagheri, N., Ghorbanian, S.A., Hallajisani, A., Poorkarimi, S., 2013. A new adsorption isotherm model of aqueous solutions on granular activated carbon. World J. Model. Simul. 9, 243–254.
Smith, K.A., Hao, J., Li, S.K., 2009. Effects of ionic strength on passive and iontophoretic transport of cationic permeant across human nail. Pharm. Res. 26, 1446–1455. https://doi.org/10.1007/s11095-009-9854-x.
Tan, D., Yuan, P., Annabi-Bergaya, F., Liu, D., Wang, L., Liu, H., He, H., 2014. Loading

and in vitro release of ibuprofen in tubular halloysite. Appl. Clay Sci. 96, 50–55.
Vaz, S., 2016. Sorption behavior of the oxytetracycline antibiotic to two Brazilian soils. Chem. Biol. Technol. Agric. 3, 6. https://doi.org/10.1186/s40538-016-0056-6.
Vergaro, V., Abdullayev, E., Lvov, Y.M., Zeitoun, A., Cingolani, R., Rinaldi, R., Leporatti, S., 2010. Cytocompatibility and uptake of halloysite clay nanotubes. Biomacromolecules 11, 820–826.
Vinokurov, V.A., Stavitskaya, A.V., Chudakov, Y.A., Ivanov, E.V., Shrestha, L.K., Ariga, K., Darrat, Y.A., Lvov, Y.M., 2017. Formation of metal clusters in halloysite clay nanotubes. Sci. Technol. Adv. Mater. 18, 147–151. https://doi.org/10.1080/14686996.2016.1278352.
Vithanage, M., Rajapaksha, A.U., Tang, X., Thiele-Bruhn, S., Kim, K.H., Lee, S.-E., Ok, Y.S., 2014. Sorption and transport of sulfamethazine in agricultural soils amended with invasive-plant-derived biochar. J. Environ. Manage. 141, 95–103.
Wang, B., Lv, X.-L., Feng, D., Xie, L.-H., Zhang, J., Li, M., Xie, Y., Li, J.-R., Zhou, H.-C., 2016. Highly stable Zr (IV)-based metal–organic frameworks for the detection and removal of antibiotics and organic explosives in water. J. Am. Chem. Soc. 138, 6204–6216.
Weber, W.J., Morris, J.C., 1963. Kinetics of adsorption on carbon from solution. J. Sanit. Eng. Div. 89, 31–60.
WHO, 2012. Pharmaceuticals in Drinking-water. https://www.who.int/water_sanitation_health/publications/2012/pharmaceuticals/en/.
Xie, A., Dai, J., Chen, X., Ma, P., He, J., Li, C., Zhou, Z., Yan, Y., 2016. Ultrahigh adsorption of typical antibiotics onto novel hierarchical porous carbons derived from renewable lignin via halloysite nanotubes-template and in-situ activation. Chem. Eng. J. 304, 609–620. https://doi.org/10.1016/j.cej.2016.06.138.
Xu, T., Zheng, F., Chen, Z., Ding, Y., Liang, Z., Liu, Y., Zhu, Z., Fong, H., 2019. Halloysite nanotubes sponges with skeletons made of electrospun nanofibers as innovative dye adsorbent and catalyst support. Chem. Eng. J. 360, 280–288. https://doi.org/10.1016/j.cej.2018.11.233.
Yu, L., Wang, H., Zhang, Y., Zhang, B., Liu, J., 2016. Recent advances in halloysite nanotube derived composites for water treatment. Environ. Sci. Nano 3, 28–44.
Yuan, P., Tan, D., Annabi-Bergaya, F., 2015. Properties and applications of halloysite nanotubes: recent research advances and future prospects. Appl. Clay Sci. 112–113, 75–93. https://doi.org/10.1016/j.clay.2015.05.001.
Zahidah, K.A., Kakooei, S., Ismail, M.C., Bothi Raja, P., 2017. Halloysite nanotubes as nanocontainer for smart coating application: a review. Prog. Org. Coat. 111, 175–185. https://doi.org/10.1016/j.porgcoat.2017.05.018.
Zeng, X., Zhong, B., Jia, Z., Zhang, Q., Chen, Y., Jia, D., 2019. Halloysite nanotubes as nanocarriers for plant herbicide and its controlled release in biodegradable polymers composite film. Appl. Clay Sci. 171, 20–28. https://doi.org/10.1016/j.clay.2019.01.021.
Zhang, Y., Yang, H., 2012. Co 3 O 4 nanoparticles on the surface of halloysite nanotubes. Phys. Chem. Miner. 39, 789–795.
Zhang, Y., Cai, X., Xiong, W., Jiang, H., Zhao, H., Yang, X., Li, C., Fu, Z., Chen, J., 2014. Molecular Insights into the pH-Dependent Adsorption and Removal of Ionizable Antibiotic Oxytetracycline by Adsorbent Cyclodextrin Polymers. PLoS One 9, e86228. https://doi.org/10.1371/journal.pone.0086228.
Zhao, Y., Abdullayev, E., Vasiliev, A., Lvov, Y., 2013. Halloysite nanotubule clay for efficient water purification. J. Colloid Interface Sci. 406, 121–129. https://doi.org/10.1016/j.jcis.2013.05.072.